Optical confinement methods for continued scaling of CMOS image sensor pixels

Christian C. Fesenmaier, Yijie Huo, and Peter B. Catrysse*

Department of Electrical Engineering, Stanford University, Stanford, CA 94305 USA
**Corresponding author: pcatryss@stanford.edu*

Abstract: The pixels that make up CMOS image sensors have steadily decreased in size over the last decade. This scaling has two effects: first, the amount of light incident on each pixel decreases, making optical efficiency, i.e., the collection of each photon, more important. Second, diffraction comes into play when pixel size approaches the wavelength of visible light, resulting in increased spatial optical crosstalk. To address these two effects, we investigate and compare three methods for guiding incident light from the microlens down to the photodiode. Two of these techniques rely on total internal reflection (TIR) at the boundary between dielectric media of different refractive indices, while the third uses reflection at a metal-dielectric interface to confine the light. Simulations are performed using a finite-difference time-domain (FDTD) method on a realistic 1.75-μm pixel model for on-axis as well as angled incidence. We evaluate the optical efficiency and spatial crosstalk performance of these methods compared to a reference pixel and find significant (10%) improvement for the TIR designs with properly chosen parameters and nearly full spatial crosstalk elimination using metal to confine the light. We also show that these improvements are comparable to those achieved by thinning the image sensor stack.

OCIS codes: (040.1490) Cameras; (050.1755) Computational electromagnetic methods; (230.7370) Waveguides; (130.2790) Guided waves

References and links

1. P. B. Catrysse, and B. A. Wandell, "Roadmap for CMOS image sensors: Moore meets Planck and Sommerfeld," Proc. SPIE **5678**, 1-13 (2005).
2. H. Rhodes, G. Agranov, C. Hong, U. Boettiger, R. Mauritzson, J. Ladd, I. Karasev, J. McKee, E. Jenkins, and W. Quinlin, "CMOS imager technology shrinks and image performance," IEEE Workshop on Microelectronics and Electron. Devices 7-18 (2004).
3. F. Xiao, J. E. Farrell, and B. A. Wandell, "Psychophysical thresholds and digital camera sensitivity: the thousand-photon limit," Proc. SPIE **5678**, 75-84 (2005).
4. P. B. Catrysse, B. A. and Wandell, "Optical efficiency of image sensor pixels," J. Opt. Soc. Am. A **19**, 1610-1620 (2002).
5. P. B. Catrysse, X. Liu, and A. El Gamal, "QE reduction due to pixel vignetting in CMOS image sensors," Proc. SPIE **3965**, 420–430 (2000).
6. G. Agranov, V. Berezin, and R. H. Tsai, "Crosstalk and microlens study in a color CMOS image sensor," IEEE Trans. Electron. Dev. **50**, 4-11 (2003).
7. C. H. Koo, H. K. Kim, K. H. Paik, D. C. Park, K. H. Lee, Y. K. Park, C. R. Moon, S. H. Lee, S. H. Hwang, and D. H. Lee, "Improvement of crosstalk on 5M CMOS image sensor with 1.7 x1.7 μm pixels," Proc. SPIE **6471**, 15 (2007).
8. D. N. Yaung, S. G. Wuu, H. C. Chien, T. H. Hsu, C. H. Tseng, J. S. Lin, J. J. Chen, C. H. Lo, C. Y. Yu, C. S. Tsai and C. S. Wang, "Air-gap guard ring for pixel sensitivity and crosstalk improvement in deep sub-micron CMOS image sensor," IEEE Intl. Electron. Devices Meeting 16.5 (2003).
9. T. H. Hsu, Y. K. Fang, D. N. Yaung, S. G. Wuu, H. C. Chien, C. H. Tseng, L. L. Yao, W. D. Wang, C. S. Wang, and S. F. Chen, "A high-efficiency CMOS image sensor with air gap in situ MicroLens (AGML) fabricated by 0.18-μm CMOS technology," IEEE Electron. Device Lett. **26**, 634-636 (2005).
10. T. H. Hsu, Y. K. Fang, C. Y. Lin, S. F. Chen, C. S. Lin, D. N. Yaung, S. G. Wuu, H. C. Chien, C. H. Tseng, and J. S. Lin, "Light guide for pixel crosstalk improvement in deep submicron CMOS image sensor," IEEE Electron. Device Lett. **25**, 22-24 (2004).
11. K. B. Cho, C. Lee, S. Eikedal, A. Baum, J. Jiang, C. Xu, X. Fan, and R. Kauffman, "A 1/2.5 inch 8.1 Mpixel CMOS Image Sensor for Digital Cameras," IEEE Intl. Solid-State Circuits Conf. 508-618 (2007).

#102073 - $15.00 USD Received 2 Oct 2008; revised 18 Nov 2008; accepted 20 Nov 2008; published 25 Nov 2008

12. S. H. Lee, C. R. Moon, K. H. Paik, S. H. Hwang, J. C. Shin, J. Jung, K. Lee, H. Noh, D. Lee, and K. Kim, "The Features and Characteristics of 5-mega CMOS Image Sensor with Topologically Unique 1.7 μm x 1.7 μm Pixels," Symp. on VLSI Tech. 142-143 (2006).
13. W. G. Lee, J. S. Kim, H. J. Kim, S. Y. Kim, S. B. Hwang, and J. G. Lee, "Two-Dimensional Optical Simulation on a Visible Ray Passing through Inter-Metal Dielectric Layers of CMOS Image Sensor Device," J. Korean Phys. Soc. **47**, S434-9 (2005).
14. W. G. Lee and J. S. Kim, "Comparison of Optical Properties in Al-and Cu-BEOL of CMOS Image Sensor Devices," Electrochem. Solid-State Lett. **9**, G254-7 (2006).
15. E. D. Palik, *Handbook of Optical Constants of Solids*, (Academic Press, Orlando, 1985).
16. A. D. Rakic, A. B. Djurisic, J. M. Elazar, and M. L. Majewski, "Optical properties of metallic films for vertical-cavity optoelectronic devices," Appl. Opt **37**, 5271–5283 (1998).
17. P. B. Catrysse, and B. A. Wandell, "Integrated color pixels in 0.18-μm complementary metal oxide semiconductor technology," J. Opt. Soc. Am. A **20**, 2293-2306 (2003).
18. D. M. Hartmann, O. Kibar, and S. C. Esener, "Characterization of a polymer microlens fabricated by use of the hydrophobic effect," Opt. Lett. **25**, 975-977 (2000).
19. K. Shinmou, K. Nakama, and T. Koyama, "Fabrication of Micro-Optic Elements by the Sol-Gel Method," J. Sol-Gel Sci. and Tech. **19**, 267-269 (2000).
20. C. P. Lin, H. Yang, and C. K. Chao, "Hexagonal microlens array modeling and fabrication using a thermal reflow process," J. Micromech. Microeng. **13**, 775-781 (2003).
21. X. C. Yuan, W. X. Yu, M. He, J. Bu, W. C Cheong, H. B. Niu, and X. Peng, "Soft-lithography-enabled fabrication of large numerical aperture refractive microlens array in hybrid SiO–TiO sol-gel glass," Appl. Phys. Lett. **86,** 114102 (2005).
22. A. Taflove, S. C. Hagness, *Computational electrodynamics: the finite-difference time-domain method*, (Artech House, Boston, 2000).
23. OptiFDTD, Optiwave Systems, Inc.
24. J. Vaillant, A. Crocherie, F. Hirigoyen, A. Cadien, and J. Pond, "Uniform illumination and rigorous electromagnetic simulations applied to CMOS image sensors," Opt. Express **15**, 5494-5503 (2007).
25. E. Hecht, *Optics*, (Pearson, San Francisco, 2002).
26. A. R. Afshar, and A. Thetford, "An experiment to measure frustrated total internal reflection," Eur J. Physiol. **3**, 72-74 (1982).
27. H. Raether, *Surface plasmons on smooth and rough surfaces and on gratings*, (Springer-Verlag, New York, 1988).
28. S. Iwabuchi, Y. Maruyama, Y. Ohgishi, M. Muramatsu, N. Karasawa, and T. Hirayama, "A Back-Illuminated High-Sensitivity Small-Pixel Color CMOS Image Sensor with Flexible Layout of Metal Wiring," IEEE Intl. Solid-State Circuits Conf. 1171-1178 (2006).
29. T. Joy, S. Pyo, S. Park, C. Choi, C. Palsule, H. Han, C. Feng, S. Lee, J. McKee, P. Altice, C. Hong, C. Boemler, J. Hynecek, M. Louie, J. Lee, D. Kim, H. Haddad, and B. Pain, "Development of a Production-Ready, Back-Illuminated CMOS Image Sensor with Small Pixels," Intl. Electron. Devices Meeting 1007-1010 (2007).

1. Introduction

The quality of images captured using complementary metal oxide semiconductor (CMOS) image sensors has steadily increased in recent years. Today, high-end digital single lens reflex (SLR) cameras are increasingly equipped with high spatial resolution CMOS sensors. Cellular telephones constitute the largest market for sensors at the low-end, where CMOS imagers are ideally suited to meet size and cost restrictions. Given these constraints, CMOS technology scaling has been applied mainly to increase spatial resolution by reducing pixel size. This scaling trend has some profound implications on pixel performance, in general, and optical performance, in particular, since the input (light) does not scale with technology.

Figure 1 shows illustrations of a typical three-dimensional (3D) pixel structure in a deep-submicron CMOS process and identifies the major pixel components that light interacts with before it is converted into electrical charge. Photons are incident on the top, where the microlens is located, and are converted into electron-hole pairs in the substrate, where the photodiode is defined.

#102073 - $15.00 USD Received 2 Oct 2008; revised 18 Nov 2008; accepted 20 Nov 2008; published 25 Nov 2008

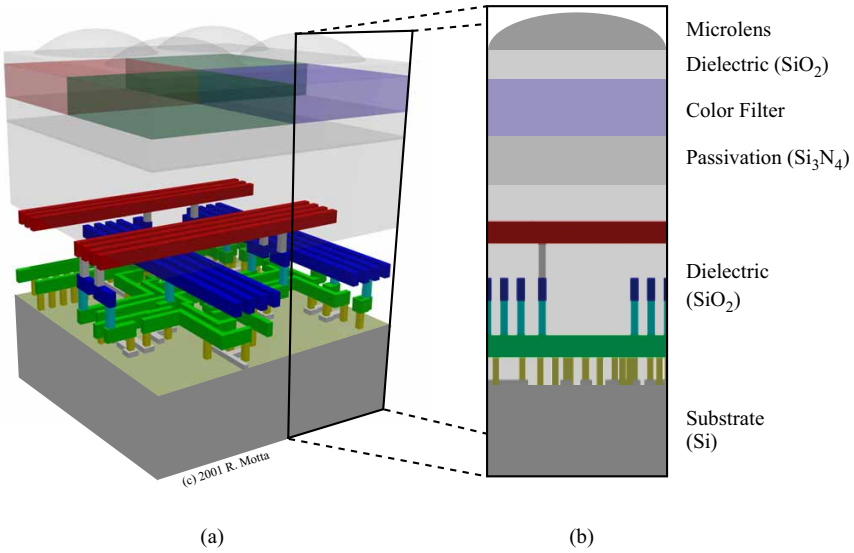

Fig. 1. (a). Three-dimensional (3D) structure of a typical four-pixel unit cell of a CMOS image sensor with a red-green-green-blue Bayer color filter array. (b) Single pixel side view, including the microlens, color filter, passivation layer, dielectric layers, metal interconnects, and silicon substrate.

Scaling of the lateral pixel size first reduces the amount of light incident on each pixel and puts an upper bound on the photodiode signal [1, 2]. Even for a perfect pixel, i.e., one that collects and converts all incident photons into electrons, there is a limit to pixel size based on fundamental photon shot noise considerations. Psychophysical experiments have shown that a signal-to-noise ratio of about 30 dB, equivalent to 1000 photons per pixel, is needed to give the visual impression of a noise-free image [3]. For realistic pixels, collection and conversion is less than perfect. Decreasing pixel size leads to additional loss of photons due to reflection, scattering, and diffraction in the region between the microlens at the pixel surface and the photodiode in the silicon substrate. This is characterized by an optical efficiency [4, 5]. Second, as pixel size approaches the wavelength of visible light, diffraction causes a sharp increase in the amount of light that reaches adjacent photodiodes, known as spatial optical crosstalk [6]. The result of crosstalk is erroneous signal at neighboring pixels, degrading resolution and color reproduction. Other types of crosstalk include spectral crosstalk, in which light that should have been blocked by a color filter manages to pass through, and electrical crosstalk, in which photo-generated electrons travel to adjacent pixels through the silicon substrate. It has been shown that spectral and electrical crosstalk contribute significantly to the total amount of crosstalk [7]. In this paper, however, we focus on spatial (optical) crosstalk as it is the most drastically affected by shrinking pixel dimensions. We note that any light collected by an adjacent pixel is also lost from the intended pixel and that methods to reduce crosstalk should also increase the optical efficiency of the intended pixel.

To minimize the adverse effects resulting from pixel scaling, we investigate three methods for guiding incident light from the microlens down to the photodiode. We examine their dependence on key design parameters, compare their performance to improvements achieved by thinning the optical stack, and comment on the feasibility of their implementation in modern CMOS image sensors.

#102073 - $15.00 USD Received 2 Oct 2008; revised 18 Nov 2008; accepted 20 Nov 2008; published 25 Nov 2008

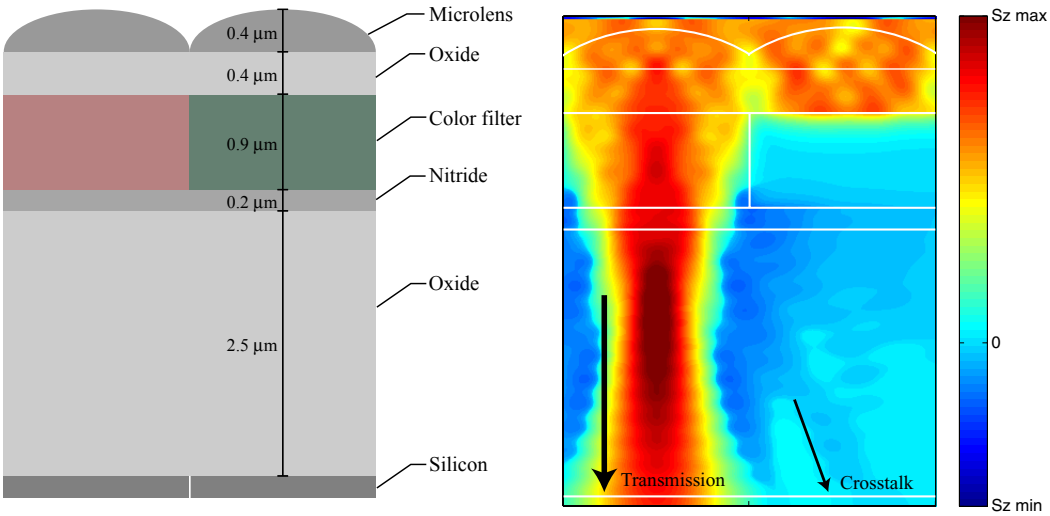

Fig. 2. (a). Two-dimensional (2D) pixel model with layer materials and thicknesses. (b). Electromagnetic field simulation result showing energy flow toward the photodiode (z-component of the Poynting vector, S_z) with significant diffraction effects, reducing optical efficiency (transmission) and leading to spatial crosstalk even at normal incidence.

2. Pixel light guiding methods

A functional pixel is comprised of several elements as detailed in Fig. 2(a). Incident light first passes through a plano-convex microlens to help focus the light in the center of the pixel. Underneath the microlens is a silicon oxide layer that separates it from the color filter in the next layer and provides a suitable surface for microlens formation. Below that, a thin silicon nitride passivation layer is followed by a thick oxide that makes up the bulk of the pixel thickness and provides support and isolation for the metal interconnects. Finally at the bottom of the pixel is the silicon substrate where a photodiode is formed and the light is absorbed.

The goal of placing light guides within pixels is to simultaneously confine light inside each pixel, increasing optical efficiency, and to prevent leakage out of the pixel, reducing optical crosstalk [Fig. 2(b)]. To guide the light from the pixel surface to the photodiode, we rely on two distinct optical effects: total internal reflection (TIR) at the boundary between a high refractive index core and low refractive index cladding, and reflection at a metal-dielectric interface. For TIR to occur, the light must be incident on the interface at an angle θ from the normal less than a critical angle, which is defined as

$$\theta_c = \cos^{-1}\left(\frac{n_{cladding}}{n_{core}}\right) \tag{1}$$

where $n_{cladding}$ and n_{core} are the refractive indices of cladding and core, respectively. The ratio of the core index over the cladding index is known as the index contrast. A higher index contrast yields a higher critical angle, leading to TIR for a greater range of angles.

One way of achieving a large index contrast is to etch away thin sections of the oxide surrounding the active pixel area that are then sealed, creating air gaps as in Fig. 3(a). The air in these pockets acts as a low-index (n = 1) cladding around a silicon dioxide (n ≈ 1.46) core. This structure has been fabricated for multiple pixel sizes from 2.8-4.0 µm and it was shown experimentally that it can appreciably increase efficiency and reduce crosstalk, especially for smaller pixels [8, 9]. For a 2.8 µm pixel, crosstalk was reduced by 64% at normal incidence and 89% at 20° incidence compared to a normal structure without air gaps [9].

#102073 - $15.00 USD Received 2 Oct 2008; revised 18 Nov 2008; accepted 20 Nov 2008; published 25 Nov 2008

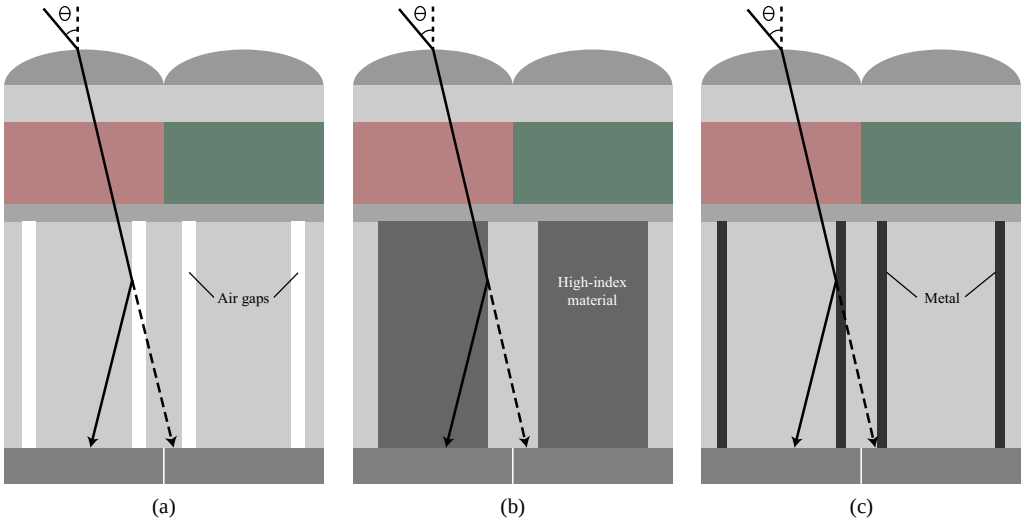

Fig. 3. Two-pixel cross-sections of the (a) low-index cladding, (b) high-index core, and (c) metal cladding light guiding methods. The solid line represents the transmitted ray, while the dashed line represents the light path without the guide.

Similarly, the central pixel area can be etched and replaced with a high-index material to create the core region, as illustrated in Fig. 3(b). Hsu *et al*. explored this design using oxides with only slightly different refractive indices [10]. Even with a very small index contrast (less than 2%), they experimentally observed improved efficiency and a 30% decrease in crosstalk at 10° incidence for a 3.0 μm pixel.

The third method we investigate is based on the reflection of light at a metal-dielectric interface. Here, we apply an optically thick metal film as the cladding that confines the light inside each pixel [Fig. 3(c)]. Unlike the previous two guides, metals are lossy, so they may introduce additional absorption while light propagates in the light guide. To our knowledge, this method has not been examined in the literature.

3. Methodology

In this section, we explain the models for the pixel and three light guides, which consist of two-dimensional (2D) pixel cross-sections with associated geometry and materials. We then identify optical efficiency and optical crosstalk as performance metrics and detail the electromagnetic simulation technique and pixel analysis procedures.

3.1 Pixel model

We use a pixel pitch of 1.75 μm because, at the time of publication, it is the smallest pixel size currently in volume production [11, 12]. The pixel height is based on typical thicknesses for microlenses, color filters, and dielectric stacks for CMOS backend technology in three-metal-layer pixels. We also evaluate two- and one-metal-layer pixels with a smaller pixel height. A reasonable area fill factor of 47% corresponding to a linear photosensitive region in the central 1.2 μm of the pixel, is introduced to realistically reproduce the behavior of an actual pixel, where the photodiode occupies only a fraction of the total pixel area [2]. Pixel designs vary greatly, especially in terms of metal interconnects. Simulating every type of pixel layout is beyond the scope of this paper. Given that metal interconnects are typically routed outside the optical path for light at low angles of incidence (i.e. for pixels near the center of the sensor), we omit metal interconnects in our simulations. For light at high angles of incidence (i.e. for pixels near the edges of the sensor), unshifted metal lines can act to block the light from reaching the intended photodiode. By omitting them, the results represent the optimal performance achievable where pixel vignetting is not taking place.

#102073 - $15.00 USD Received 2 Oct 2008; revised 18 Nov 2008; accepted 20 Nov 2008; published 25 Nov 2008

The microlens is represented by a truncated spherical surface with a fixed radius of curvature and thickness. All other layers are modeled as thin dielectric films with fixed thicknesses that are approximated based on examples in literature [13, 14]. The dielectric material properties are described by refractive indices obtained from Palik [15]. Metal optical constants are modeled using a Drude free-electron model [16, 17]. For the non-standard materials, specifically the microlens and color filter, approximations are made based on a literature survey [18-21]. We note that only the silicon substrate, color filter material, and metal cladding are modeled as absorptive materials.

3.2 Light guide models

For each light guiding method, we vary a key design parameter affecting performance. Leakage of light can occur for small cladding thicknesses, so for the low-index cladding method, simulations are performed for air gap thicknesses of 0.05, 0.1, 0.15, and 0.2 μm. The critical angle and therefore the degree of light confinement depends on the index contrast, so simulations are performed for high-index core refractive indices of 1.5, 1.55, 1.6, and 1.7. The metal is kept at 0.1 μm thick (optically thick or non-transparent), but we use aluminum and tungsten to predict the effectiveness of different CMOS compatible metals. The light guide core widths, defined as the distance from the inner edges of the light guide, are kept equal to the active pixel area of 1.2 μm regardless of the parameter variations. Although the shapes of the guides may vary in real structures, they are approximated here as rectangular.

3.3 Performance metrics

To properly evaluate the simulation results, we introduce two measures of pixel performance. Optical efficiency, also called transmission, is defined as the fraction of optical power incident on the surface of each pixel that reaches the intended photodiode at the silicon substrate [4]. Optical crosstalk is defined as the average fraction of optical power incident on each pixel that reaches the photodiodes in adjacent pixels.

3.4 Finite-difference time-domain method

The finite-difference time-domain (FDTD) method is a powerful approach for explicitly determining the electric and magnetic fields at every point when electromagnetic radiation (light) is incident on a pixel structure. FDTD models the propagation of light by discretizing, in both time and space, and numerically solving the time-dependent Maxwell's equations. By stepping forward in very short time increments and alternately solving for the electric and magnetic fields, a steady-state solution can be reached for continuous wave (CW) calculations. This type of explicit calculation is necessary due to the small dimensions of the pixel structure, which are well below the size at which ray optics and scalar wave optics break down [22].

For our simulations, we use a commercial FDTD implementation [23]. The incident light is modeled as a continuous plane wave excitation in air just above the microlens surface. Plane wave illumination is an approximation that does not take into account the finite f-number of the imaging optics, which would lead to a distribution of incidence angles. This subject was more rigorously discussed by Vaillant *et al.* [24]; in our simulations we study the changes in performance with angle and design parameters by restricting the distribution of incoming light to one angle. Optical efficiency and crosstalk measurements are taken just below the oxide-silicon interface. These values are obtained by taking the discrete Fourier transform of the time trace after the transient response due to the onset of the CW excitation has left the simulation domain and the system has settled into a steady-state while being driven by the CW excitation. The resulting fields are used to calculate the Poynting vector S_z, which is integrated over the central 1.2 μm pixel width to obtain the total steady-state power delivered to the photodiode [17]. We also assume 100% quantum efficiency, i.e. complete conversion of photons to electrons, for light entering the photodiode area at the silicon interface and do not consider photon absorption deeper in the substrate.

#102073 - $15.00 USD Received 2 Oct 2008; revised 18 Nov 2008; accepted 20 Nov 2008; published 25 Nov 2008

We choose to focus on the red part of the visible spectrum since diffraction effects are most severe for longer wavelengths. The pixel of interest in this study therefore has a red color filter and is placed in the center of a multi-pixel array with completely absorbing "black" color filters above all other pixels that act as a masking layer. Simulations with varying number of pixels showed that a five-pixel array is the best compromise to limit simulation time and discount boundary layer effects. Anisotropic perfectly matched absorbing boundary layers are used at all domain edges to prevent reflections. The simulation grid size is set to 10 nm as this is a reasonable minimum element position increment and yields more than 15 steps per wavelength in the highest index medium. The time step is determined using the Courant-Friedrichs-Levy condition [22].

Incidence angles from 0 to 30° in 5° increments are simulated to emulate the illumination at pixels located in different positions in the array and survey the effectiveness of the designs across the sensor. Both transverse electric (TE, electric field perpendicular to the pixel cross-section) and transverse magnetic (TM, magnetic field perpendicular) simulations are performed for each design. The stated results are the average of the two polarizations, as light from a typical scene is unpolarized. We limit the simulations to a small range of wavelengths (645-655 nm). The 10 nm range is sampled at 2 nm steps and results are incoherently averaged to remove any effects associated with (coherent) interference oscillations in the transmission spectrum. Over this narrow range, material optical properties are approximately constant, so refractive index data at 650 nm is used for all simulations.

4. Results

In this section, we describe the microlens optimization for the designs and the results of the design parameter analysis.

4.1 Microlens optimization

The microlens on top of each image sensor pixel performs the important function of concentrating light onto the pixel photodetector to minimize the amount of light incident on non-photosensitive regions of the pixel substrate [1]. We optimize the radius of the microlens at normal incidence to the nearest 0.1 μm using FDTD while holding its thickness constant at 0.4 μm. We select the ratio of average crosstalk at the nearest-neighbor pixels to the optical efficiency of the intended pixel as merit function. Each of the light guides has the same aperture width, but because pixel structure changes affect the focusing behavior of the light, we optimize each design individually.

In addition to focusing the light, microlenses also redirect the light path. This is necessary because the angle of incident light increases as the distance from the center of the sensor increases, such that light will travel to adjacent pixels unless the microlens is shifted toward the sensor center [1, 6]. We optimize the microlens shifts for each of the designs at each non-zero angle of incidence. The color filter array also must be shifted; this offset is calculated based on the microlens shift considering a line of sight from the edges of the microlens either to the edges of the active pixel area for the reference pixel, or to the light guide aperture. Shifts are optimized to within the nearest 0.1 μm, again using the crosstalk to optical efficiency ratio as the figure of merit.

4.2 Low-index cladding

We now examine the effects of changing design parameters on the performance of the light guiding methods. For comparison, we also show the results for the reference pixel in each case. For the low-index cladding light guide, we change the thickness of the air gap between 0.05 and 0.2 μm in 0.05 μm increments. FDTD simulations are used to calculate the energy flow toward the photodiode (z-component of the Poynting vector S_z) for angles of incidence between 0 and 30°. Figure 4 shows an example calculation for the 0.05 and 0.2 μm air gap thicknesses for light with a 30° incidence angle. The plots show a higher amount of light

#102073 - $15.00 USD Received 2 Oct 2008; revised 18 Nov 2008; accepted 20 Nov 2008; published 25 Nov 2008

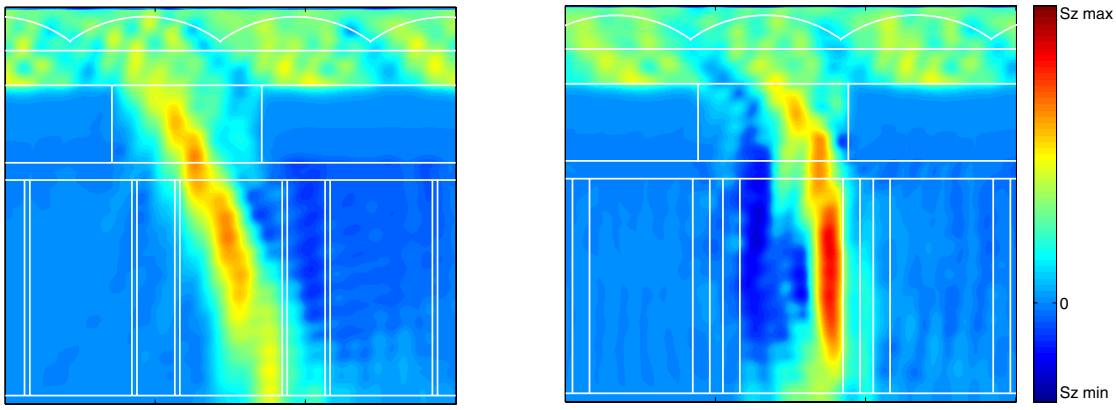

(a) (b)

Fig. 4. Poynting vector plots depicting energy flow toward the photodiode for the (a) 0.05 μm thick and (b) 0.2 μm thick low-index cladding designs for light with a 30° incidence angle and a wavelength of 651 nm. Only the center three pixels are shown and the boundaries between different materials are outlined. The scale has been modified nonlinearly to bring out detail in the regions of lower energy flow.

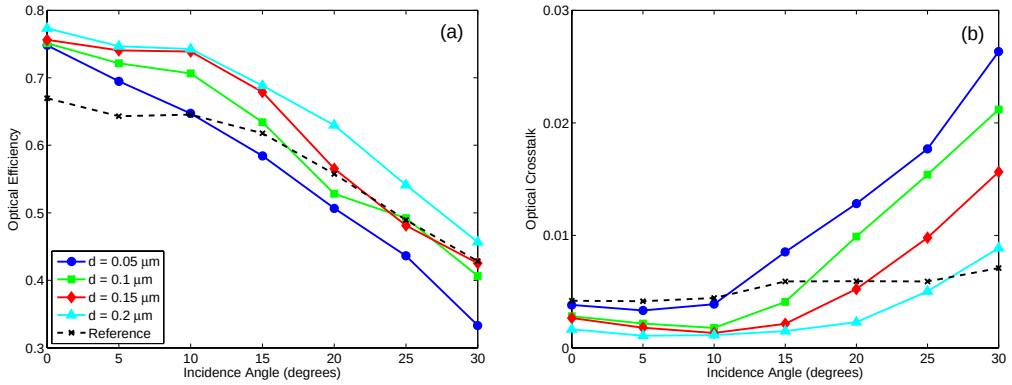

Fig. 5. Plots of (a) optical efficiency and (b) crosstalk for the four low-index cladding designs and the reference pixel as a function of incidence angle. Legend indicates results for different air gap thicknesses and reference pixel in both plots.

leakage for the thinner air gap due to frustrated TIR, which occurs when the evanescent wave in the air gap couples to the dielectric across the gap [25]. Since the light must pass through two air gaps to reach the adjacent pixel core, there is some light trapped between pixels. This light is not counted as signal for either pixel. We also note the difference in optimal microlens shifts resulting in a change in light position at the light guide aperture. The regions of negative energy flow in the Poynting vector plots represent energy moving away from photodiode due to reflection that occurs mainly at the oxide-silicon interface.

#102073 - $15.00 USD Received 2 Oct 2008; revised 18 Nov 2008; accepted 20 Nov 2008; published 25 Nov 2008

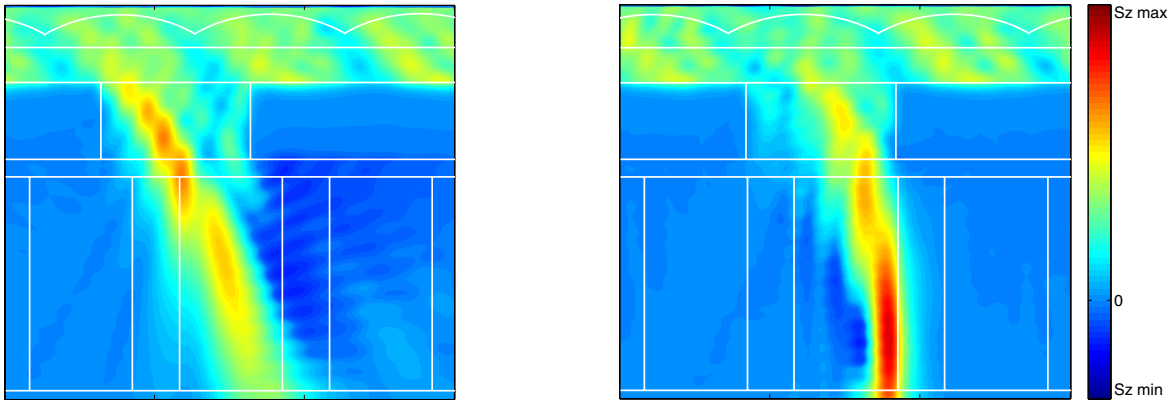

(a) (b)

Fig. 6. Poynting vector plots depicting energy flow toward the photodiode for the (a) n = 1.5 and (b) n = 1.7 high-index core designs for light with 30° incidence angle and wavelength of 651 nm. Only the center three pixels are shown and the boundaries between materials are outlined. The scale has been modified nonlinearly to bring out detail in the regions of lower energy flow.

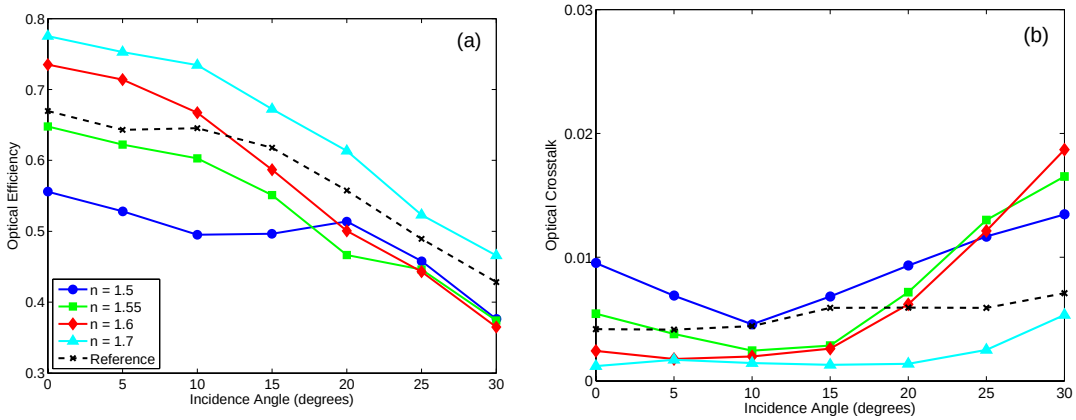

Fig. 7. Plots of (a) optical efficiency and (b) crosstalk for the four high-index core designs and the reference pixel as a function of incidence angle. Legend indicates results for different core indices and reference pixel in both plots.

Figure 5 plots optical efficiency and crosstalk as a function of incidence angle for the low-index cladding designs. From 0 to 10°, the light guides outperform the reference pixel in terms of optical efficiency and crosstalk as they collect and confine the light that would otherwise diffract. Optical efficiency is very similar among the designs in this range since the aperture size is kept constant as the air gap width changes. The exception is the thinnest air gap (0.05 μm) design, which fails almost immediately. This agrees well with theoretical calculations for frustrated TIR [26].

Above 10°, a breakdown in confinement occurs for all light guides, resulting in a drop in optical efficiency. It is also evident in the increased crosstalk for the 0.05 and 0.1 μm thick designs. The crosstalk is in fact worse than the reference due to stray reflections caused by light that is not accepted into the light guide. Crosstalk for the 0.15 μm design, however, only significantly increases above 15°, while the 0.2 μm air gap design only breaks down above

#102073 - $15.00 USD Received 2 Oct 2008; revised 18 Nov 2008; accepted 20 Nov 2008; published 25 Nov 2008

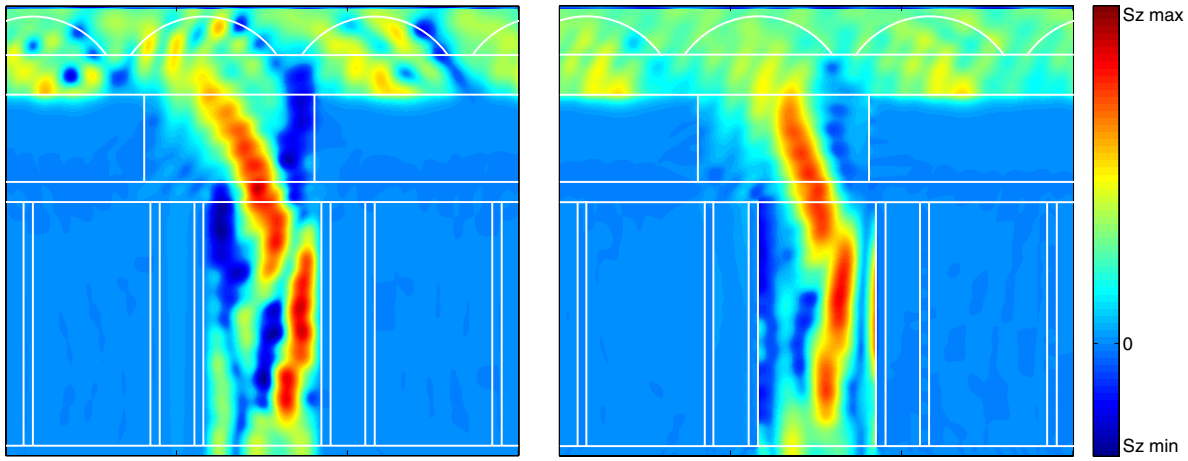

(a) (b)

Fig. 8. Poynting vector plots depicting energy flow toward the photodiode for the aluminum light guide design for (a) TE and (b) TM polarizations for light with a 30° incidence angle and a wavelength of 651 nm. Only the center three pixels are shown and the boundaries between materials are outlined. The scale has been modified nonlinearly to bring out detail in the regions of lower energy flow.

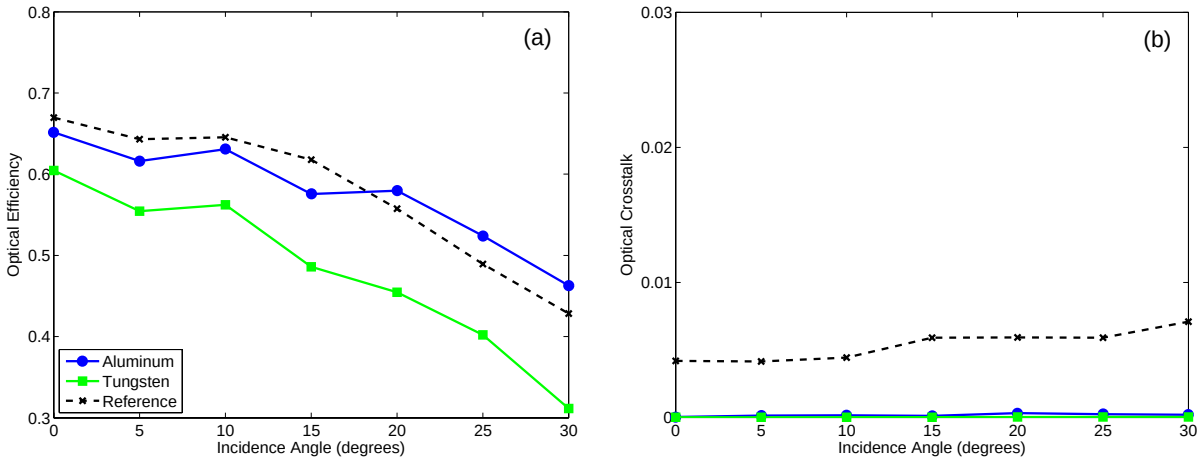

Fig. 9. Plots of (a) optical efficiency and (b) crosstalk for the metal (TE and TM polarizations) and the reference pixel as a function of incidence angle. Legend indicates results for different polarizations and reference pixel in both plots.

20° incidence. We note that the expected correlation between decreased optical efficiency and increased crosstalk is not always observed. This can be explained by noting that some light leaves the pixel core, but impinges on the silicon outside the active photodiode areas in the dead zone between pixels. This same effect was observed experimentally by Agranov *et al.* [6].

4.3 High-index core

For the high-index core designs, we vary the refractive index of the core material. Figure 6 shows two example FDTD simulations for the n = 1.5 and 1.7 high-index cores at 30°. There is significant light leakage outside the pixel core for the lower-index design because the incident angle exceeds the critical angle (about 13° in this case) and TIR does not take place. On the other hand, the higher-index core visibly holds the light inside the pixel center.

#102073 - $15.00 USD Received 2 Oct 2008; revised 18 Nov 2008; accepted 20 Nov 2008; published 25 Nov 2008

Figure 7 plots the optical efficiency and crosstalk results as a function of angle. In this light guide, the light travels through the varying material, leading to differences in optical efficiency for normal incidence. The increase in optical efficiency for higher indices is attributed to a reduced amount of light reflection at the silicon-oxide interface due to better index matching between the core material and silicon ($n \approx 4$). Optical efficiency steadily decreases for all the designs as angle increases and more of the light reaches the inactive area between the pixels. Once the incident angle becomes greater than the critical angle of the waveguide, the light is able to reach the neighboring photodiode and crosstalk sharply increases. For the $n = 1.5$ case, crosstalk begins to rise at 15°, which agrees with the critical angle of 13.3°. Similarly, crosstalk only significantly increases at 20° for the $n = 1.55$ case in agreement with its critical angle of 19.6°. The $n = 1.7$ case, however, only begins to show an increase in crosstalk at 30°, just below its critical angle.

4.4 Metal cladding

Figures 8(a) and 8(b) show the Poynting vector for light at 30° angle of incidence on the metal cladding structure for TE and TM polarizations, respectively. There is nearly no energy flow outside the pixel core. An interesting phenomenon arises for the TM polarization in which part of the light is "attracted" to the metal-dielectric interface. This is most likely due to the formation of a surface plasmon-polariton that propagates along the metal, confining the energy near the metal surface. This effect is particularly strong for flat metal surfaces that lack the roughness to allow the surface plasmon-polariton to scatter away from the metal-dielectric surface [27].

Figure 9 plots the optical efficiency and crosstalk results for the metal waveguide. While optical efficiency for the TE polarization is excellent, it is significantly lower for TM because the light propagation in close vicinity to the metal results in absorption by the lossy metal. The optical efficiency of the tungsten light guide is significantly lower than the aluminum due to increased absorption in the less conductive metal. Optical efficiency for the TM polarization is nearly constant for all angles; Poynting vector plots show that this is due to surface plasmon formation and field confinement regardless of angle. Crosstalk is more than ten times less than the reference and invariant with angle for either polarization and for both materials because there is no penetration through the metal.

4.5 Light guide comparison

Figure 10 summarizes the change in optical efficiency and crosstalk from the reference for all simulated designs at normal and 30° incidence (blue and red bars, respectively). We observe an on-axis optical efficiency of 0.67 for the reference pixel, i.e. a third of the light incident on each pixel is lost. We attribute the loss to absorption in the color filter, reflection from the dielectric stack, and diffraction sending the light away from the active pixel area. As expected, optical efficiency decreases and crosstalk increases as angle increases.

All the low-index cladding designs yield optical efficiencies that are at least 10% greater than the reference at normal incidence. At high angles of incidence only the thickest air gap design is comparable to the reference with a 7% improvement in optical efficiency, but a 25% increase in crosstalk. The high-index core method suffers from significant interference effects that make the $n = 1.5$ and $n = 1.55$ cases worse than the reference for on-axis light. At 30°, only the highest-index core light guide improves over the reference in both optical efficiency (9% increase) and crosstalk (25% decrease).

Some designs perform worse than the reference, especially for the highest angle. This is the result of practical limitations on microlens shift: if the microlens is shifted too far, the light will miss the light guide aperture. For those methods that cannot contain the light, however, this shift is not enough to ensure that the light does not reach the active area of the adjacent photodiode after it leaves the light guide. It is vital, therefore, that for light guide designs to be useful near the edges of the sensor, where steeper incidence angles are encountered, it must have a minimum level of confinement or it will actually increase crosstalk and decrease optical efficiency compared to the reference. For sensors operating at up to 30° incidence, this

#102073 - $15.00 USD Received 2 Oct 2008; revised 18 Nov 2008; accepted 20 Nov 2008; published 25 Nov 2008

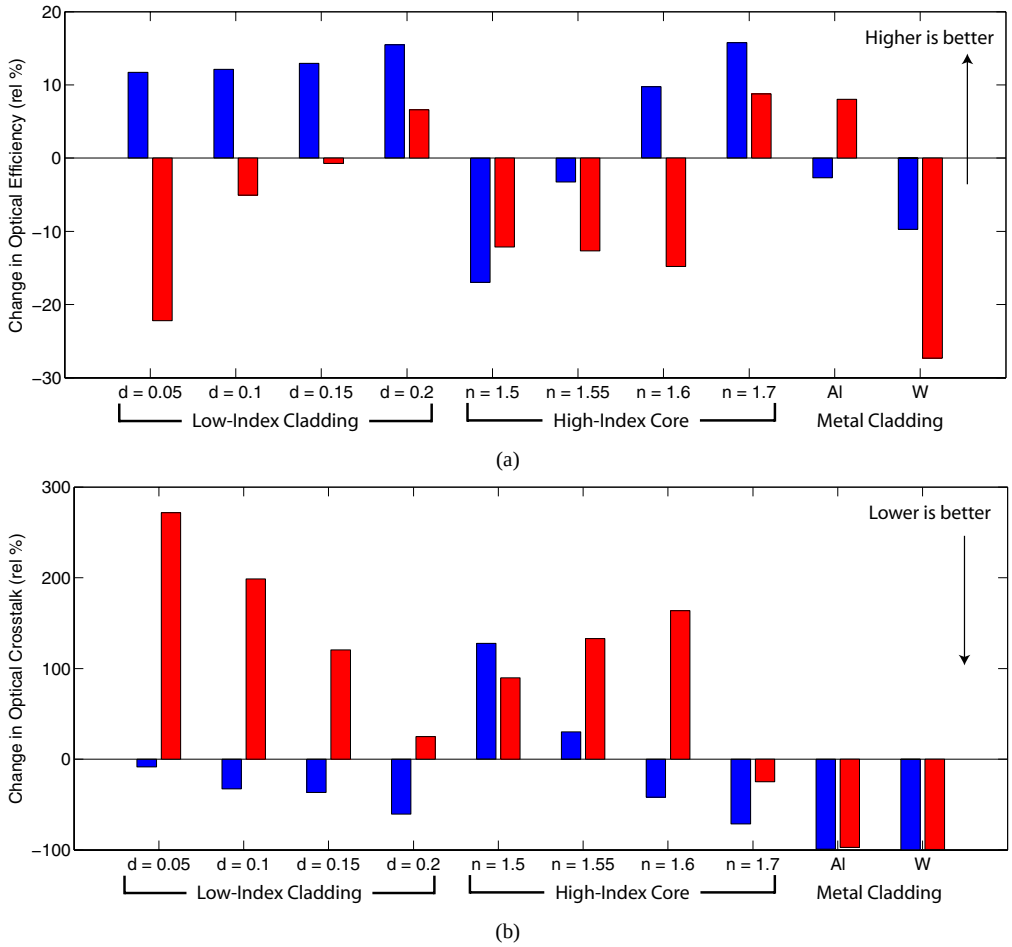

Fig. 10. Bar graphs showing relative percentage change in (a) optical efficiency and (b) crosstalk from the reference for all simulated light guide designs at normal (blue bars) and 30° (red bars) incidence.

limitation would rule out the low-index claddings thinner than 0.2 μm as well as all but the highest index (n = 1.7) core design. For angles of 10° or less, the low-index cladding is beneficial for both optical efficiency and crosstalk regardless of the air gap thickness and is therefore the best choice for low angles.

The metal cladding designs show vastly superior crosstalk reduction (over 90% for all angles). Optical efficiency for aluminum was comparable to the reference pixel, ranging from a 7% decrease to 8% gain over all angles, while tungsten suffers from high absorption losses in the metal and therefore has significantly lower optical efficiency (greater than 10% decrease for all angles).

4.6 Light guide performance comparison to stack height reduction

The optical problems associated with reducing pixel size have also stimulated research into reducing the distance between the microlens and photodiode by eliminating one or more interconnect layers. This modification allows the thick dielectric layer that supports and isolates the metal lines to be thinned. To compare the effects of this change, we simulate pixels corresponding to two and one metal layers with oxide thicknesses of 1.83 and 1.16 μm. These thicknesses yield on-axis optical efficiencies equal to the reference pixel in the one-dimensional approximation where the microlens is a flat layer. All other layers remain the

#102073 - $15.00 USD Received 2 Oct 2008; revised 18 Nov 2008; accepted 20 Nov 2008; published 25 Nov 2008

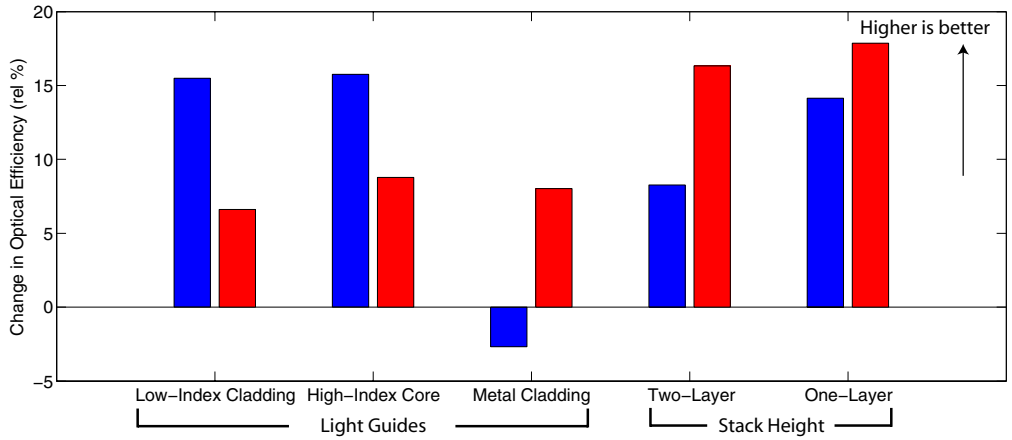

(a)

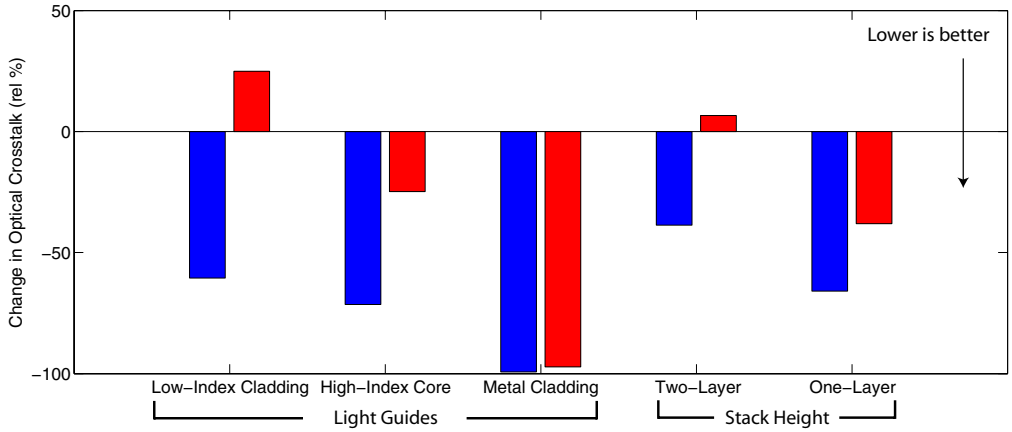

(b)

Fig. 11. Bar graphs showing relative percentage change in (a) optical efficiency and (b) crosstalk from the reference for the best of each light guide design and the thinned stacks at normal (blue bars) and 30° (red bars) incidence.

same and as before no interconnects are included. The microlenses for these thinner stack designs were optimized using methods identical to those used for the reference design. In Fig. 11, we present the change in optical efficiency and crosstalk from the reference for the two- and one-layer designs as well as the best of each light guiding method at normal and 30° incidence (blue and red bars respectively).

The shorter stacks show a marked improvement in optical efficiency (8% and 14% for two- and one-metal layer thicknesses, respectively), which, as expected, increases as the oxide is thinned. This is attributed to less spreading of light due to a shorter path from the microlens to the photodiode such that more light is focused onto the active pixel area. The increase in optical efficiency for both thinned stacks is less than the best light guiding designs for on-axis light. For light incident at 30°, however, the thinner stacks outperform the light guides by about 10% as the latter suffer from difficulties in getting all the light into the guide and confining it at high angles. The crosstalk trends suffer from higher-order diffraction fringes, which change in location with the pixel height. The two-layer pixel does not offer significant improvement, however, over the reference or light guides for a 1.75 μm pixel used in this study. The one-layer design performs comparably to the best high-index core light guide, reducing crosstalk by 66% and 38% at normal and 30° incidence compared to the reference.

#102073 - $15.00 USD Received 2 Oct 2008; revised 18 Nov 2008; accepted 20 Nov 2008; published 25 Nov 2008

5. Conclusions and discussion

The low-index cladding designs improve optical efficiency by about 10% at normal incidence compared to a reference pixel without waveguide. Their crosstalk performance, on the other hand, is worse at high angles of incidence even for the thickest air gaps. This may prove to be serious drawback for this type of waveguide, in addition to the fact that little room is left for interconnects as the gaps become thicker or the pixel becomes smaller. The metal cladding designs show vastly superior crosstalk reduction (over 90% for all angles), but the optical efficiency is at best comparable the reference pixel. These designs should be considered for applications where it is more important to reduce crosstalk rather than it is to achieve the highest possible optical efficiency. On the other hand, the highest-index core light guide improves over the reference in both optical efficiency (9% increase) and crosstalk (25% decrease). Therefore it may be the most likely candidate for most applications if a viable material can be found. There is also the possibility of combining the two TIR methods in the same sensor to provide even better confinement. While the plasmon-polariton effect in the metal cladding design offers the potential of subwavelength waveguiding, the absorption losses need to be reduced by appropriate design of the metal interfaces. The widespread implementation of such high-aspect ratio vertically-oriented metal layers is presently not feasible in a standard CMOS process and would require the development of new fabrication techniques. Given the use of metals such as tungsten for vertical vias, however, this capability is not far out of reach.

Future developments such as a reduction in the number of metal layers, leading to a shorter dielectric stack, will help to alleviate the problem of decreasing optical efficiency and increasing crosstalk, but cannot provide a complete solution and introduce restrictions on interconnect design. More drastic changes to the pixel structure, such as backside illumination through thinning of the silicon substrate, have the potential to further decrease the distance from the pixel surface to the photodiode and therefore reduce the effects of diffraction. These new structures, however, present significant engineering challenges and considerable advances are required before they will be ready for production [28, 29].

While this study focused on one specific pixel size (1.75 μm), image sensor pixels will probably continue to scale. Further research should be done to evaluate how the efficacy of the proposed light guiding methods will change with pixel size. Regardless of which approach is taken, as pixel sizes become smaller to the point of being comparable to the wavelength of visible light, more attention must be given to optically isolating pixels in order to preserve image quality.

Acknowledgments

This work was supported through a generous gift from MagnaChip Semiconductor Ltd. The authors thank B. A. Wandell for fruitful discussions, and B. Fowler, A. El Gamal, J. Farrell, H. Haddad, C. Feng, T. Joy, I. Patrick, J. Hynecek, A. Theuwissen, and R. Motta for critical feedback. We also thank R. Motta for the original 3D pixel drawings used in Fig. 1.

#102073 - $15.00 USD Received 2 Oct 2008; revised 18 Nov 2008; accepted 20 Nov 2008; published 25 Nov 2008